AGU ADVANCING EARTH AND SPACE SCIENCE

Geophysical Research Letters

RESEARCH LETTER
10.1029/2020GL091028

Atlantic Deep Water Formation Occurs Primarily in the Iceland Basin and Irminger Sea by Local Buoyancy Forcing

Tillys Petit[1], **M. Susan Lozier**[1], **Simon A. Josey**[2], **and Stuart A. Cunningham**[3]

[1]School of Earth and Atmospheric Sciences, Georgia Institute of Technology, Atlanta, GA, USA, [2]National Oceanography Centre, Southampton, UK, [3]Scottish Association for Marine Science, Oban, UK

Key Points:
- New observations reveal Atlantic Subpolar Gyre deep water is formed primarily in the Irminger and Iceland basins by local buoyancy forcing
- The deep water formed by buoyancy forcing in winter is not entirely exported the following months; a portion is stored in those basins
- The transformation and subsequent export of deep water southward are twice as large in winter 2014–2015 than in winter 2015–2016

Supporting Information:
- Supporting Information S1

Correspondence to:
T. Petit,
tillys.petit@gatech.edu

Citation:
Petit, T., Lozier, M. S., Josey, S. A., & Cunningham, S. A. (2020). Atlantic deep water formation occurs primarily in the Iceland Basin and Irminger Sea by local buoyancy forcing. *Geophysical Research Letters*, *47*, e2020GL091028. https://doi.org/10.1029/2020GL091028

Received 28 SEP 2020
Accepted 29 OCT 2020

Abstract The Atlantic Meridional Overturning Circulation (AMOC), a key mechanism in the climate system, delivers warm and salty waters from the subtropical gyre to the subpolar gyre and Nordic Seas, where they are transformed into denser waters flowing southward in the lower AMOC limb. The prevailing hypothesis is that dense waters formed in the Labrador and Nordic Seas are the sources for the AMOC lower limb. However, recent observations reveal that convection in the Labrador Sea contributes minimally to the total overturning of the subpolar gyre. In this study, we show that the AMOC is instead primarily composed of waters formed in the Nordic Seas and Irminger and Iceland basins. A first direct estimate of heat and freshwater fluxes over these basins demonstrates that buoyancy forcing during the winter months can almost wholly account for the dense waters of the subpolar North Atlantic that are exported as part of the AMOC.

Plain Language Summary The Atlantic Meridional Overturning Circulation (AMOC) is a key mechanism in the climate system, as it contributes to the uptake and storage of anthropogenic CO_2 in the deep ocean. As global warming continues apace, climate scientists are concerned with the possibility of a slowing AMOC due to changes in deep water formation at high latitudes in the North Atlantic. Although wintertime conditions over the Labrador Sea have long been considered a strong predictor of downstream AMOC change, recent results in the subpolar North Atlantic have revealed that the volume of deep waters formed in the Labrador Sea is small compared with the waters carried in the AMOC, creating an unresolved question as to the source of deep waters that compose the lower AMOC limb. Here, we combine a collection of observations from the subpolar gyre and Nordic Seas to show that the Iceland Basin and Irminger Sea are the main sources for the lower limb. Additionally, we reveal that the production of deep waters can almost entirely be accounted for by wintertime air-sea fluxes over those basins and that some of the dense waters formed via convection are stored in the Irminger and Iceland basins in subsequent months.

1. Introduction

The Atlantic Meridional Overturning Circulation (AMOC) delivers warm and salty waters in its upper limb to the North Atlantic subpolar gyre and Nordic Seas, where they are transformed into large volumes of cold and fresh waters in the AMOC lower limb via air-sea buoyancy loss in wintertime (Lozier, 2010). The prevailing hypothesis for the sources of the AMOC lower limb has been that approximately half was provided by Nordic Sea waters flowing over the sills into the Iceland and Irminger basins (Isachsen et al., 2007; Mauritzen, 1996), and half formed via convection in the Labrador Sea (Bailey et al., 2005; Schmitz & McCartney, 1993; Worthington, 1976). However, results from a relatively new observational program have challenged that view by providing evidence that the strength of Labrador Sea convection contributes minimally to the total overturning of the subpolar gyre (Lozier et al., 2019). As such, the sources for waters of the AMOC lower limb have come into question.

The Overturning in the Subpolar North Atlantic Program (OSNAP) array was deployed in the summer of 2014 to provide continuous measurement of the AMOC at subpolar latitudes (Lozier et al., 2017). The array is composed of two sections: OSNAP West at the Labrador Sea entrance and OSNAP East, which extends from the southeast tip of Greenland to the Scottish shelf (Figure 1a). OSNAP observations through May 2016 (Lozier et al., 2019) show that the overturning across OSNAP East (15.6 ± 0.8 Sv) exceeds the

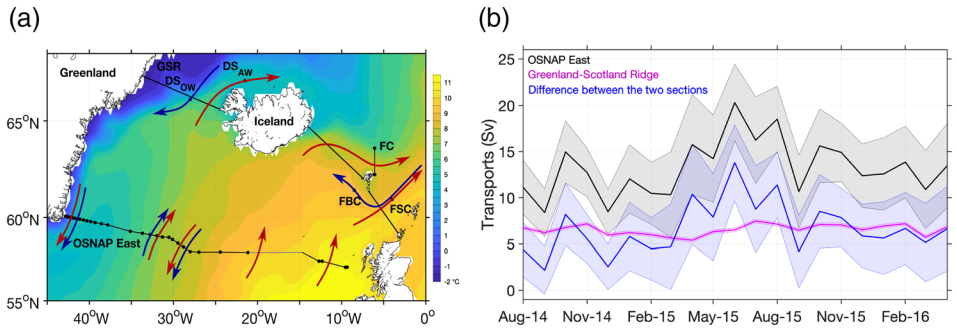

Figure 1. OSNAP East and GSR observations. (a) Map of sea surface temperature (°C) during the OSNAP period showing mooring locations along OSNAP East and GSR for (1) Atlantic inflows at Denmark Strait (DS_{AW}), Faroe-Shetland Current (FSC), and Faroe Current (FC) and (2) overflows at Denmark Strait (DS_{OW}) and Faroe-Bank Chanel (FBC). The gray line at OSNAP East denotes the glider survey region. Red and blue arrows depict upper and lower flows, respectively. (b) Thirty-day mean transports (positive southward) integrated over the lower layer at OSNAP East (black line) and GSR (magenta line) and their difference (blue line). Shading indicates uncertainty in the means. The two layers are separated by the 30-day varying isopycnal of the AMOC at OSNAP East, noted σ_{MOC}. See section 2for details on the uncertainty estimates.

overturning across OSNAP West (2.1 ± 0.3 Sv). A small overturning in the Labrador Sea was also estimated from composite hydrographic sections during 1990–1997 (Pickart & Spall, 2007), suggesting that weak overturning at OSNAP West is not an anomaly of the shorter OSNAP observational period.

To identify the source of the relatively large volume of the AMOC lower limb flowing across OSNAP East (separated from the upper limb by the AMOC isopycnal, σ_{MOC}; section 2.1), we compare continuous transport measurements across the Greenland-Scotland Ridge (GSR) with those across OSNAP East (Figure 2). We find that the mean transport across GSR (−6.6 ± 0.4 Sv) cannot explain that across OSNAP East (−13.2 ± 3.8 Sv), a result suggested by Sarafanov et al. (2012) from an analysis of summer hydrographic sections. Similarly, waters flowing across GSR in the AMOC upper limb (7.4 ± 0.4 Sv) are half of those flowing

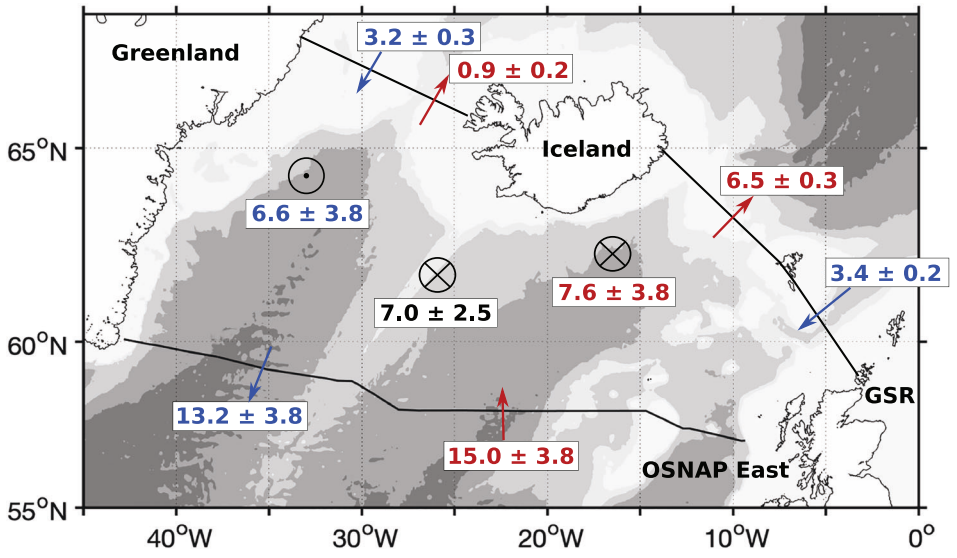

Figure 2. Overturning and buoyancy forcing between OSNAP East and GSR. Volume budget of the upper (red) and lower (blue) layers between GSR and OSNAP East (Sv). Within-layer transports are averaged over the OSNAP period. Circle with a central dot indicates the volume of water received in the lower layer from the upper layer estimated from the volume budget of the lower layer; circles with crosses indicate export of water from the upper layer to the lower layer estimated from the volume budget of the upper layer and from the averaged transformation across σ_{MOC} (black, unit Sv). Bathymetry is shaded for 500, 1,000, 2,000, and 3,000 m. Note that the red and blue arrows across the OSNAP line are placeholders for a number of significant currents that compose the upper and lower limbs.

across OSNAP East (15.0 ± 3.8 Sv). The overturning variability across OSNAP East can also not be attributed to the deep waters flowing southward across GSR (Figure 1b) since the transport variability for the deep GSR waters (±2 Sv) is small in comparison to that across OSNAP East (±12 Sv).

Thus, the overall goal of this study is to ascertain the mechanism responsible for producing deep waters in the eastern subpolar North Atlantic. Specifically, we explore whether transformation of surface waters by air-sea fluxes of heat and freshwater in the region can account for the lower (upper) fluxes of 6.6 ± 3.8 Sv (7.6 ± 3.8 Sv) needed to close the mass budget between OSNAP East and GSR (Figure 2). To complement this exploration, we also assess the impact of buoyancy forcing over the Labrador and Nordic Seas during the OSNAP period.

2. Materials and Methods

2.1. The OSNAP East Observations

The OSNAP East array consists of 32 moorings from the southeast tip of Greenland to the Scottish shelf (Lozier et al., 2017). The distance between moorings (Figure 1) varies from 9.6 km at the Greenland shelf (42.5°W/60°N) to 389 km above the Hatton-Rockall Basins (14–21°W/58°N). Geostrophic velocity fields are estimated from continuous temperature, salinity, and velocity measurements of the OSNAP moorings, combined with other observations (Argo profiling floats, OSNAP gliders and CTD stations, WORLD Ocean Atlas 2013 climatology, and current meter velocities) for the period between August 2014 and May 2016. Salinity, temperature, and geostrophic velocity fields are gridded with a horizontal resolution of ~25 km and a vertical resolution of 20 m (Li et al., 2017). Here, we used the gridded transports estimated from the 30-day mean geostrophic velocities (Table S1 in the supporting information).

The transports were integrated in the upper and lower layer at OSNAP East, which are separated by the 30-day varying AMOC isopycnal, σ_{MOC}. The AMOC isopycnal is defined each month as the density at the maximum of the overturning stream function in density space. It ranges from 27.38 kg m^{-3} in December 2014 to 27.76 kg m^{-3} in September 2014 with an average $\overline{\sigma \mathrm{MOC}}$ of 27.55 kg m^{-3}.

Statistical uncertainties for the AMOC are estimated from Monte Carlo simulations (Thomson & Emery, 2014) and were applied for the transports across OSNAP East. The statistical uncertainty was estimated as 3.8 Sv for the upper and lower layers.

2.2. Exchanges Across the GSR

We used transports across the GSR provided by the AtlantOS consortium (Bringedal et al., 2018). The transports are estimated for the upper and lower layers from moorings and hydrographic stations (Figure 1a). Note that the density limit between the layers is defined as 27.80 kg m^{-3} at the GSR.

The upper layer includes northward Atlantic water through the Denmark Strait (Jonsson & Valdilarsson, 2012), the Faroe Current (Hansen et al., 2015), and the Faroe-Shetland Chanel (Berx et al., 2013) (Figure 1a). Observations for this layer run through the period 1994–2014. Because the transports do not span the entire OSNAP period, monthly averages were used to create averaged time series for the rest of the OSNAP period. Indeed, we assume that the mean states prevail through 2014–2016, as these flows are steady over time (Table S1).

The lower layer is composed of southward Denmark Strait Overflow Water (DSOW) at the Denmark Strait (Jochumsen et al., 2017) and Iceland-Scotland Overflow Water (ISOW) at the Faroe-Bank Chanel (Hansen et al., 2016; Hansen & Østerhus, 2007) (Figure 1a). In that layer, the averaged ISOW transports through the Wyville-Thomson Ridge and the Iceland-Faroe Ridge of 0.8 Sv (Hansen et al., 2018) and 0.4 Sv (Sherwin, 2010), respectively, were included to the exchanges through the Faroe-Bank Channel.

The standard error for the GSR transports is computed as $E_{GSR} = \frac{std(T)}{\sqrt{n}}$, where $std(T)$ is the standard deviation of the transports and n is the effective degree of freedom computed from the autocorrelation function of the time series. Because the density limit between the upper and lower layers, defined as 27.80 kg m^{-3} at the GSR, is denser than $\overline{\sigma \mathrm{MOC}}$ = 27.55 kg m^{-3}, an uncertainty associated with the net middepth exchange across the GSR is added to the cross-ridge flows (Sarafanov et al., 2012). The uncertainty in the sum of the upper and lower transports is shared equally between the western and eastern sides of Iceland and applied

to each cross-ridge transport. The final error was estimated as 0.3 Sv for the southward DSOW and the exchanges at the Faroe-Shetland Channel, and as 0.2 Sv for the southward ISOW and the exchanges of Atlantic water through the Denmark Strait during the 21 months of OSNAP observations.

2.3. Atmospheric Reanalysis

We use National Centers for Environmental Prediction (NCEP)/National Center for Atmospheric Research (NCAR) atmospheric reanalysis (Kalnay et al., 1996) and European Centre for Medium Range Weather Forecasts Reanalysis 5 (ERA5) atmospheric reanalysis (Poli et al., 2016) to estimate air-sea heat and freshwater fluxes over the area defined between OSNAP East and GSR. These are combined with monthly fields of subsurface salinity between August 2014 and May 2016 to compute the transformations of outcropped waters. Subsurface salinities at 5-m depth were derived from EN4.2.1 (Good et al., 2013) and, as for the NCEP/NCAR fluxes, were subsampled onto the ERA5 grid of 30 km.

2.4. Transformation of Outcropped Waters

The transformation of surface water by air-sea fluxes is computed using a well-developed method based on a linearized version of the equation of state (Speer & Tziperman, 1992; Tziperman, 1986; Walin, 1982). Assuming steady state, the amount of water transformed across an isopycnal outcrop toward higher or lower densities by net heat and freshwater fluxes is computed for each month and each isopycnal σ following the equations below. A local surface density flux is integrated over time and the area of the density outcrop to yield the transformation, F (Figure S1). When σ does not outcrop in a given month, F is set to zero.

$$F(\sigma^*) = \frac{1}{\Delta\sigma}\iint\left[-\frac{\alpha}{C_P}Q + \beta\frac{S}{1-S}(E-P)\right]\Pi(\sigma)dx\,dy$$

where

$$\Pi(\sigma) = \begin{cases} 1 & \text{for} |\sigma - \sigma^*| \le \dfrac{\Delta\sigma}{2} \\ 0 & \text{elsewhere} \end{cases}.$$

α is the thermal expansion coefficient, β is the haline contraction coefficient, S is the subsurface salinity, C is the specific heat, H is the net heat flux into the ocean, and E and P are the evaporation and precipitation, respectively. The bin size in density is set at $\Delta\sigma = 0.2$ kg m^{-3} to avoid noise at finer intervals (Speer & Tziperman, 1992).

Statistical uncertainty for the transformation is estimated as the standard error for the monthly transformations across σ_{MOC}: $r = \dfrac{std(F\sigma)}{\sqrt{n}}$, where $std(F_\sigma)$ is the standard deviation of the monthly transformations across σ_{MOC} over the 21 months of OSNAP observations and n is the effective degree of freedom computed from the autocorrelation function of the time series. This error was estimated at 2.5 Sv in the Irminger Sea and Iceland Basin between OSNAP East and GSR.

3. Results

3.1. Densification Due to Buoyancy Forcing Over the OSNAP Period

The transport difference between deep flows across GSR and OSNAP East (6.6 ± 3.8 Sv; Figure 2 and Table S1) is similar to that found (9.6 ± 3.5 Sv) using composites of summertime hydrographic sections at GSR and at 59.5°N (Chafik & Rossby, 2019), the latter of which roughly aligns with OSNAP East. In that study, the authors attribute the difference between the volume of deep water coming over GSR and that exported at 59.5°N to entrainment and subsequent densification of intermediate water by the overflow waters. Other studies highlight buoyancy forcing, rather than entrainment, as the primary mechanism for densification in the Irminger Sea (Brambilla et al., 2008; Brambilla & Talley, 2008), though a quantification of its impact has yet to be made. That quantification is the focus of this section.

According to the method in Speer and Tziperman (1992) and described in section 2.4, we compute the transformation of outcropped waters to densities exceeding σ_{MOC}, the AMOC isopycnal separating the upper and

lower limbs, during the 21 months of OSNAP data. Our estimate yields a transformation of 7.0 ± 2.5 Sv over the area bounded by OSNAP East and GSR (Figure 2), which matches remarkably well with the mean overturning estimated by the volume budget in both layers (6.6 ± 3.8 Sv for the lower layer; 7.6 ± 3.8 Sv for the upper layer). Thus, the volume of deep water exported from the Irminger and Iceland basins across OSNAP East can be accounted for by overflow waters across the GSR and by water mass formation through buoyancy loss over this region. The entrainment of ambient water by the overflow does not seem to play a major role in the transformation of upper waters to densities larger than σ_{MOC}. Nevertheless, the entrainment is not negligible in the subsequent transformation of the deep waters within the lower limb of the AMOC (Dickson & Brown, 1994; van Aken & de Jong, 2012), and thus on the deep water properties exported southward.

The strongest transformation of surface water to the mean AMOC density ($\overline{\sigma MOC} = 27.55$ kg m^{-3}) occurs along the boundary current in the Irminger Sea and north of 59°N in the region over the Reykjanes Ridge (Figure 3b), which is consistent with Brambilla et al. (2008). The importance of these areas for transformation is highlighted by the black crosses that denote regions where the 27.55 kg m^{-3} isopycnal outcropped during all 8 months of the 2014–2015 and 2015–2016 winters. With such persistent outcropping, these "hot spots" play a key role in the transformation of light to dense waters between OSNAP East and GSR. In contrast, transformation is relatively weak over the Hatton-Rockall Basin and does not occur over the Rockall Trough at this density.

However, the transformation to densities that define the lower AMOC limb is understood to be the final stage in water mass formation across the subpolar gyre. Thus, we also examine the spatial pattern of transformation across 27.35 kg m^{-3} (Figure 3a), which we consider the density of subpolar mode waters found in the eastern region of the subpolar gyre that are "preconditioned" to become the dense waters of the lower limb further downstream (Brambilla & Talley, 2008; Talley & McCartney, 1982; Thierry et al., 2008). Strong transformation to this density is found in the southeastern part of the Iceland Basin, whereas weak transformation is observed over the Irminger Sea. Consistent with previous publications (Brambilla et al., 2008; Desbruyères et al., 2019), our analysis shows that wintertime convection in the Iceland Basin, Hatton-Rockall Basin, and northern Rockall Trough provides critical preconditioning for the deep waters of the AMOC lower limb.

We now extend our transformation analysis to the Labrador and Nordic Seas in order to understand if estimates of overturning in those basins can similarly be explained by buoyancy forcing. For the Labrador Sea, we find a water mass transformation of 1.5 ± 0.7 Sv to densities exceeding 27.70 kg m^{-3} (Figure S1), the AMOC density at OSNAP West, which compares reasonably well with the recently published estimate (Lozier et al., 2019) of overturning in that basin of 2.1 ± 0.3 Sv. Turning to the Nordic Seas, we have already noted that 6.6 ± 0.4 Sv of overflow waters ($\sigma_0 > 27.80$ kg m^{-3}) joins the Irminger and Iceland basins through the GSR during the OSNAP period. Our calculation of the transformation to densities greater than 27.80 kg m^{-3} in the Nordic Seas (from GSR to Fram Strait and the Barents Sea Opening) during the same period yields 4.7 ± 1.5 Sv (Figure S1), which agrees with the finding of Isachsen et al. (2007) that the primary production of the dense water flowing across the GSR occurs in the Nordic Seas. Thus, for all basins where we expect waters that comprise the deep limb of the AMOC to be formed, we find that the volume of waters exported can largely be explained by buoyancy loss over these basins in the winter months.

In earlier work using coupled models, a surface-forced overturning was estimated for the entire North Atlantic north of a given latitude and compared against the model's "actual" overturning computed using velocity fields (Grist et al., 2009; Josey et al., 2009). Josey et al. (2009) found the surface-forced estimate was best matched to the actual by averaging the surface-forced estimate over a number of years, for example, 6 years at 60°N and 10 years at 45°N. Desbruyères et al. (2019) found similar results using observations. In both studies, a lag is expected because of the circulation timescales over a basin-wide area. In contrast, we focus here only on the Irminger and Iceland basins and find that local surface fluxes are driving the diapycnal fluxes with little or no lag.

3.2. Temporal Variability of the Overturning in the Iceland and Irminger Basins

Over the 21 months of OSNAP observations, overturning variability between OSNAP East and GSR is large, with the 30-day means ranging from 2.2 ± 2.6 Sv in September 2014 to 13.8 ± 4.1 Sv in June 2015 (Figure 1b).

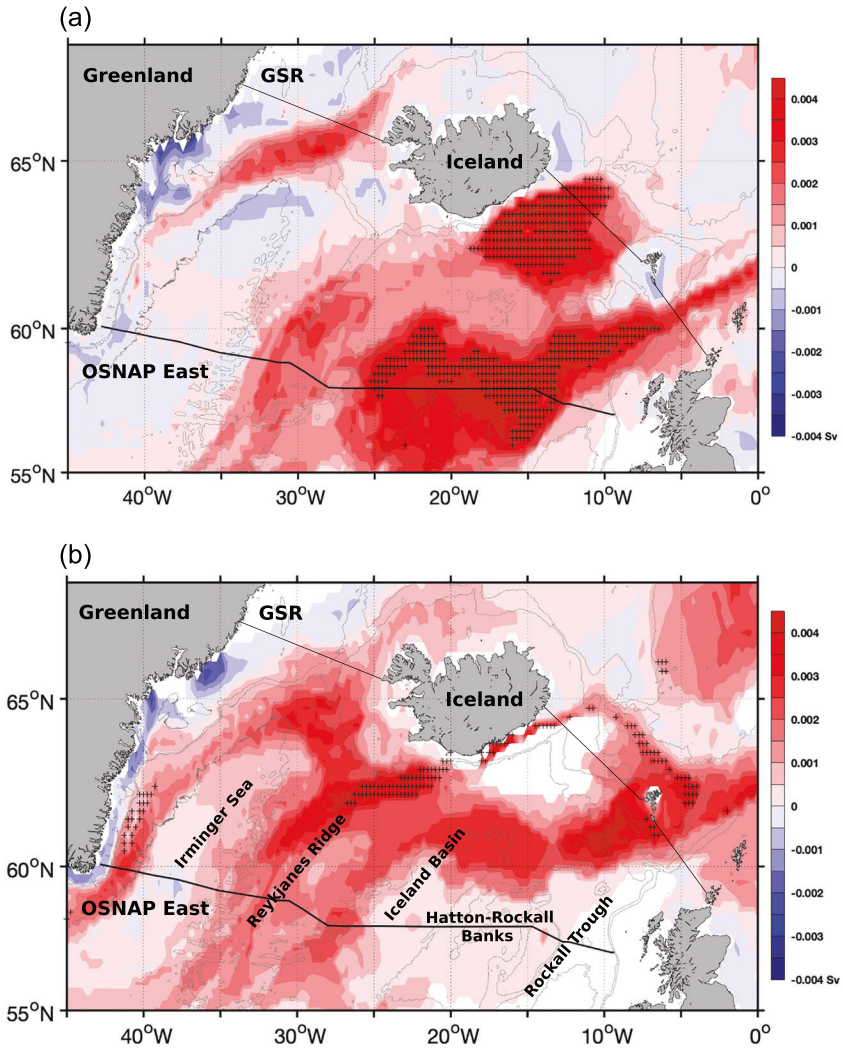

Figure 3. Spatial pattern of transformation. Transformation (Sv) at (a) 27.35 kg $m^{-3}$and (b) 27.55 kg m^{-3} over the Irminger Sea and Iceland Basin averaged over the 21-month OSNAP period and derived from the heat and freshwater fluxes of ERA5 and NCEP. Positive transformation is associated with densification to the denoted isopycnals. Black crosses indicate outcropping areas of the isopycnals during all 8 months of winter (December–March) 2014–2015 and 2015–2016. Bathymetry contours are at 500, 1,000, and 2,500 m. White indicates regions with no outcropping in any month. In addition to the Irminger Sea boundary and Reykjanes Ridge, a region of strong transformation is centered on (62°N, 10°W); however, it is not associated with persistent outcropping during all eight months of winter 2014–2015.

To further investigate this variability, the volume change for the upper and lower layers for each month is estimated by adding the net volume gain/loss due to horizontal advection and the net volume gain/loss due to transformation into/out of that layer.

Volume changes for the lower layer can be described with two steps: accumulation of water from the upper layer in winter due to densification and then subsequent export of water out of the Irminger and Iceland basins the following months (Figure 4). In winter 2014–2015, the transformation of water to densities greater than σ_{MOC} reaches a total of 29.1 Sv in January of 2015. During those winter months, the loss of water out of the lower layer is steady, but weak, with a minimum of −4.3 Sv in December 2014; thus, the layer thickens. For the upper layer, the strong densification due to buoyancy forcing overwhelms the weak advective gain such that there is a thinning of the layer during those months. Note that the thinning (volume loss) and thickening (volume gain) for the upper and lower layers, respectively, are in close agreement, with extrema in December 2014 of −24.3 Sv for the upper layer and of 24.5 Sv for the lower layer.

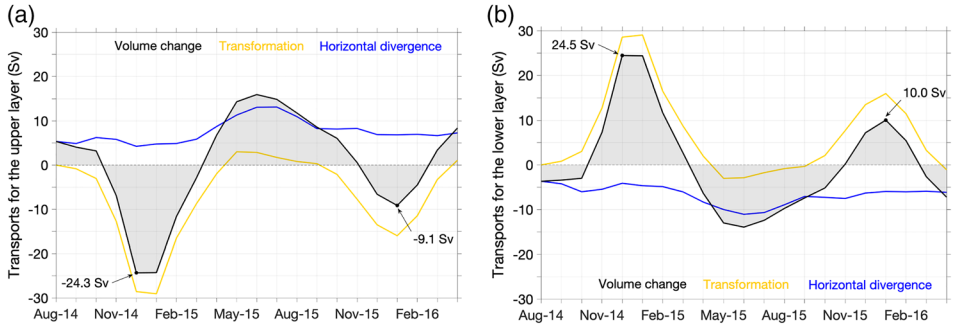

Figure 4. Monthly variability of the layer volumes. Thirty-day mean volume change (Sv) in the (a) upper and (b) lower layers between OSNAP East and GSR (black lines). The volume change is estimated by combining the transformation at the AMOC isopycnal through air-sea flux forcing (Sv, yellow lines) and the horizontal divergence of transport into each layer as estimated in Figure 1b (Sv, blue lines). The three variables are positive for inflows into the layer, such that positive transformations are associated with lightening in the upper layer and densification in the lower layer. Positive shading indicates an accumulated volume in the layer, and negative shading indicates a volume lost for the layer. The products are smoothed over 3 months. The two layers are separated by the 30-day varying isopycnal of the AMOC at OSNAP East, σ_{MOC}, which has an average of 27.55 kg m^{-3}.

After January 2015, transformation to densities greater than σ_{MOC} weakens while the net volume exported out of the basins due to advection for the lower layer reaches its maximum of −11.1 Sv in July 2015. Thus, the lower layer thins during spring to summer.

The maximum volume of water exported out of the lower layer by the horizontal flow field lags the peak of densification by 5 months. The length of this delay—between the formation of dense water and its export to the boundary current in a marginal sea, such as the Irminger Sea—is consistent with modeling studies that attribute the exchange between the convective region and the boundary current to an eddy transport mechanism (Brüggemann & Katsman, 2019; Sayol et al., 2019). The delay depends upon the location of the convection and ranges from 3 months if convection takes place along the Irminger Current to more than 12 months if it is in the interior of the Irminger Sea (Le Bras et al., 2020).

Over 1 year, the volume gain in the lower layer due to transformation exceeds the volume lost due to advection, implying that a fraction of the transformed water is stored in the Irminger and Iceland basins and not exported seasonally. From October 2014 to September 2015, 4.5 Sv is stored in the lower layer of these basins. We note that the volume accumulated in the lower layer varies from year to year (Figure 4): The accumulation is larger in winter 2014–2015 (24.5/−24.3 Sv) than in winter 2015–2016 (10.0/−9.1 Sv). Thus, the overturning variability downstream is impacted by the advection of dense water exported across OSNAP East as much as by the transformation. On longer timescales, we have an expectation that the export of waters out of the lower limb will match the transformation, or production, of the dense waters in that limb.

4. Conclusion and Implications

From the first synthesis of in situ observations (OSNAP and NACLIM) and air-sea buoyancy exchanges in each basin of the subpolar North Atlantic and the Nordic Seas, a new understanding of overturning in the eastern subpolar gyre emerges. The sources for the AMOC lower limb deep water are, in order of importance, the Irminger and Iceland basins, the Nordic Seas, and finally the Labrador Sea. This relevance stands in contrast to past studies that partitioned the deep water sources between the Nordic and Labrador Seas. We suggest that this earlier partitioning resulted from the fact that part of the deep waters formed in the Irminger and Iceland basins are carried toward the Labrador Sea via the Deep Western Boundary Current. Then, although they are further modified in the Labrador Sea and exit the basin as "Labrador Sea Water," the bulk of these waters joined the lower limb of the AMOC upstream.

Our results reveal that the production of deep water in the Irminger and Iceland basins can almost entirely be accounted for by buoyancy forcing over those basins. The close agreement between overturning and buoyancy forcing over the subpolar gyre highlights the key role of air-sea fluxes in establishing the state of the AMOC. Furthermore, considering the relatively large fraction of transformed water that is stored in

the Irminger and Iceland basins each year, an investigation into the sensitivity of the AMOC to previously observed intense interannual variability in this region (Josey et al., 2018, 2019) is warranted.

Conflict of Interest

The authors declare no competing interests.

Data Availability Statement

The data used for the conclusion of the paper are archived in data repositories. Observations at the OSNAP East section are accessible online (at https://www.o-snap.org/observations/data/), and those at the Greenland-Scotland Ridge are provided by Atlantos (http://www.oceansites.org/tma/gsr.html). The atmospheric reanalyses are freely available online (through https://www.ecmwf.int/en/forecasts/datasets/reanalysis-datasets/era5 and https://www.ncep.noaa.gov). The subsurface salinities derived from EN4.2.1 are accessible at the Met Office website (https://www.metoffice.gov.uk/hadobs/en4/download-en4-2-1.html#l09_profiles).

Acknowledgments

T. P. and M. S. L. acknowledge support from the Physical Oceanography Program of the U.S. National Science Foundation (Grant 3331843). S. A. J. acknowledges funding from the UK Natural Environment Research Council, including the North Atlantic Climate System Integrated Study program (Reference Number NE/N018044/1). S. C. U. was supported by UK NERC National Capability Programme the Extended Ellett Line and CLASS (NE/R015953/1) and NERC Large Grant UK OSNAP (NE/K010875/1) and from the European Union's Horizon 2020 Research and Innovation Programme under Grant Agreement No. 678760 (ATLAS) and No. 727852 (Blue-Action). This output reflects only the author's view, and the European Union cannot be held responsible for any use that may be made of the information contained therein.

References

Bailey, D. A., Rhines, P. B., & Häkkinen, S. (2005). Formation and pathways of North Atlantic Deep Water in a coupled ice-ocean model of the Arctic-North Atlantic Oceans. *Climate Dynamics*, *25*, 497–516. https://doi.org/10.1007/s00382-005-0050-3

Berx, B., Hansen, B., Østerhus, S., Larsen, K. M., Sherwin, T., & Jochumsen, K. (2013). Combining in situ measurements and altimetry to estimate volume, heat and salt transport variability through the Faroe-Shetland Channel. *Ocean Science*, *9*, 639–654. https://doi.org/10.5194/os-9-639-2013

Brambilla, E., & Talley, L. D. (2008). Subpolar mode water in the northeastern Atlantic: 1. Averaged properties and mean circulation. *Journal of Geophysical Research*, *113*, C04025. https://doi.org/10.1029/2006JC004062

Brambilla, E., Talley, L. D., & Robbins, P. E. (2008). Subpolar Mode Water in the northeastern Atlantic: 2. Origin and transformation. *Journal of Geophysical Research*, *113*, C04026. https://doi.org/10.1029/2006JC004063

Bringedal, C., Eldevik, T., Skagseth, Ø., Spall, M. A., & Østerhus, S. (2018). Structure and forcing of observed exchanges across the Greenland-Scotland Ridge. *Journal of Climate*, *31*, 9881–9901. https://doi.org/10.1175/JCLI-D-17-0889.1

Brüggemann, N., & Katsman, C. A. (2019). Dynamics of downwelling in an eddying marginal sea: Contrasting the Eulerian and the isopycnal perspective. *Journal of Physical Oceanography*, 3017–3035. https://doi.org/10.1175/jpo-d-19-0090.1

Chafik, L., & Rossby, T. (2019). Volume, heat, and freshwater divergences in the subpolar North Atlantic suggest the Nordic Seas as key to the state of the meridional overturning circulation. *Geophysical Research Letters*, *46*, 4799–4808. https://doi.org/10.1029/2019GL082110

Desbruyères, D. G., Mercier, H., Maze, G., & Daniault, N. (2019). Surface predictor of overturning circulation and heat content change in the subpolar North Atlantic. *Ocean Science*, *15*, 809–817. https://doi.org/10.5194/os-15-809-2019

Dickson, R., & Brown, J. (1994). The production of North Atlantic Deep Water: Sources, rates, and pathways. *Journal of Geophysical Research*, *99*, 12,319–12,341.

Good, S. A., Martin, M. J., & Rayner, N. A. (2013). EN4: Quality controlled ocean temperature and salinity profiles and monthly objective analyses with uncertainty estimates. *Journal of Geophysical Research: Oceans*, *118*, 6704–6716. https://doi.org/10.1002/2013JC009067

Grist, J. P., Marsh, R., & Josey, S. A. (2009). On the relationship between the North Atlantic Meridional Overturning Circulation and the surface-forced overturning streamfunction. *Journal of Climate*, *22*, 4989–5002. https://doi.org/10.1175/2009JCLI2574.1

Hansen, B., Larsen, K. M. H., Hátún, H., Kristiansen, R., Mortensen, E., & Østerhus, S. (2015). Transport of volume, heat, and salt towards the Arctic in the Faroe Current 1993–2013. *Ocean Science*, *11*, 743–757. https://doi.org/10.5194/os-11-743-2015

Hansen, B., Husgaro, K. M., Hátún, H., & Østerhus, S. (2016). A stable Faroe Bank Channel overflow 1995–2015. *Ocean Science*, *12*, 1205–1220. https://doi.org/10.5194/os-12-1205-2016

Hansen, B., Margretha Húsgar Larsen, K., Malskær Olsen, S., Quadfasel, D., Jochumsen, K., & Østerhus, S. (2018). Overflow of cold water across the Iceland-Faroe Ridge through the Western Valley. *Ocean Science*, *14*, 871–885. https://doi.org/10.5194/os-14-871-2018

Hansen, B., & Østerhus, S. (2007). Faroe Bank Channel overflow 1995–2005. *Progress in Oceanography*, *75*, 817–856. https://doi.org/10.1016/j.pocean.2007.09.004

Isachsen, P. E., Mauritzen, C., & Svendsen, H. (2007). Dense water formation in the Nordic Seas diagnosed from sea surface buoyancy fluxes. *Deep-Sea Research Part I: Oceanographic Research Papers*, *54*, 22–41. https://doi.org/10.1016/j.dsr.2006.09.008

Jochumsen, K., Moritz, M., Nunes, N., Quadfasel, D., Larsen, K. M. H., Hansen, B., et al. (2017). Revised transport estimates of the Denmark Strait overflow. *Journal of Geophysical Research: Oceans*, *122*, 3434–3450. https://doi.org/10.1002/2017JC012803

Jonsson, S., & Valdilarsson, H. (2012). Water mass transport variability to the North Icelandic shelf, 1994–2010. *ICES Journal of Marine Science*, *69*, 809–815. https://doi.org/10.1093/icesjms/fss024

Josey, S. A., de Jong, M. F., Oltmanns, M., Moore, G. K., & Weller, R. A. (2019). Extreme variability in Irminger Sea winter heat loss revealed by ocean observatories initiative mooring and the ERA5 reanalysis. *Geophysical Research Letters*, *46*, 293–302. https://doi.org/10.1029/2018GL080956

Josey, S. A., Grist, J. P., & Marsh, R. (2009). Estimates of meridional overturning circulation variability in the North Atlantic from surface density flux fields. *Journal of Geophysical Research*, *114*, C09022. https://doi.org/10.1029/2008JC005230

Josey, S. A., Hirschi, J. J.-M., Sinha, B., Duchez, A., Grist, J. P., & Marsh, R. (2018). The recent Atlantic cold anomaly: Causes, consequences, and related phenomena. *Annual Review of Marine Science*, *10*, 475–501. https://doi.org/10.1146/annurev-marine-121916-063102

Kalnay, E., Kanamitsu, M., Kistler, R., Collins, W., Deaven, D., Gandin, L., et al. (1996). The NCEP/NCAR 40-year reanalysis project. *Bulletin of the American Meteorological Society*, *77*, 437–471. https://doi.org/10.1175/1520-0477(1996)077<0437:TNYRP>2.0.CO;2

Le Bras, I. A.-A., Straneo, F., Holte, J., de Jong, M. F., & Holliday, N. P. (2020). Rapid export of waters formed by convection near the Irminger Sea's Western boundary. *Geophysical Research Letters*, *47*, e2019GL085989. https://doi.org/10.1029/2019GL085989

Li, F., Lozier, M. S., & Johns, W. E. (2017). Calculating the meridional volume, heat, and freshwater transports from an observing system in the subpolar North Atlantic: Observing system simulation experiment. *Journal of Atmospheric and Oceanic Technology*, *34*, 1483–1500. https://doi.org/10.1175/JTECH-D-16-0247.1

Lozier, M. S. (2010). Deconstructing the conveyor belt. *Science*, *328*, 1507–1511. https://doi.org/10.1126/science.1189250

Lozier, M. S., Bacon, S., Bower, A. S., Cunningham, S. A., de Jong, M. F., de Steur, L., et al. (2017). Overturning in the Subpolar North Atlantic Program: A new international ocean observing system. *Bulletin of the American Meteorological Society*, *98*, 737–752. https://doi.org/10.1175/BAMS-D-16-0057.1

Lozier, M. S., Li, F., Bacon, S., Bahr, F., Bower, A. S., Cunningham, S. A., et al. (2019). A sea change in our view of overturning in the subpolar North Atlantic. *Science*, *363*, 516–521. https://doi.org/10.1126/science.aau6592

Mauritzen, C. (1996). Production of dense overflow waters feeding the North Atlantic across the Greenland-Scotland Ridge. Part 1: Evidence for a revised circulation scheme. *Deep-Sea Research Part I: Oceanographic Research Papers*, *43*, 769–806. https://doi.org/10.1016/0967-0637(96)00037-4

Pickart, R. S., & Spall, M. A. (2007). Impact of Labrador Sea convection on the North Atlantic meridional overturning circulation. *Journal of Physical Oceanography*, *37*, 2207–2227. https://doi.org/10.1175/jpo3178.1

Poli, P., Hersbach, H., Dee, D. P., Berrisford, P., Simmons, A. J., Vitart, F., et al. (2016). ERA-20C: An atmospheric reanalysis of the twentieth century. *Journal of Climate*, *29*, 4083–4097. https://doi.org/10.1175/JCLI-D-15-0556.1

Sarafanov, A., Falina, A., Mercier, H., Sokov, A., Lherminier, P., Gourcuff, C., et al. (2012). Mean full-depth summer circulation and transports at the northern periphery of the Atlantic Ocean in the 2000s. *Journal of Geophysical Research*, *117*, C01014. https://doi.org/10.1029/2011JC007572

Sayol, J.-M., Dijkstra, H., & Katsman, C. (2019). Seasonal and regional variations of sinking in the subpolar North Atlantic from a high-resolution ocean model. *Ocean Science Discussions*, *15*(4), 1033-1053. https://doi.org/10.5194/os-15-1033-2019,https://os.copernicus.org/articles/15/1033/2019/

Schmitz, W. J., & McCartney, M. S. (1993). On the North Atlantic circulation. *Reviews of Geophysics*, *31*, 29–49. https://doi.org/10.1029/92RG02583

Sherwin, T. J. (2010). Observations of the velocity profile of a fast and deep oceanic density current constrained in a gully. *Journal of Geophysical Research*, *115*, C03013. https://doi.org/10.1029/2009JC005557

Speer, K., & Tziperman, E. (1992). Rates of water mass formation in the North Atlantic Ocean. *Journal of Physical Oceanography*, *22*, 93–104.

Talley, L. D., & McCartney, M. S. (1982). Distribution and circulation of Labrador sea water. *Journal of Physical Oceanography*, *12*, 1189–1205. https://doi.org/10.1175/1520-0485(1982)012<1189:DACOLS>2.0.CO;2

Thierry, V., de Boisséon, E., & Mercier, H. (2008). Interannual variability of the subpolar mode water properties over the Reykjanes Ridge during 1990–2006. *Journal of Geophysical Research*, *113*, C04016. https://doi.org/10.1029/2007JC004443

Thomson, R. E., & Emery, W. J. (2014). *Data analysis method in physical oceanography*. New York: Elsevier S.

Tziperman, E. (1986). On the role of interior mixing and air-sea fluxes in determining the stratification and circulation of the oceans. *Journal of Physical Oceanography*, *16*, 680–693. https://doi.org/10.1175/1520-0485(1986)016<0680:OTROIM>2.0.CO;2

van Aken, H. M., & de Jong, M. F. (2012). Hydrographic variability of Denmark Strait Overflow Water near Cape Farewell with multi-decadal to weekly time scales. *Deep-Sea Research Part I: Oceanographic Research Papers*, *66*, 41–50. https://doi.org/10.1016/j.dsr.2012.04.004

Walin, G. (1982). On the relation between sea-surface heat flow and thermal circulation in the ocean. *Tellus*, *34*, 187–195.

Worthington, L. V. (1976). On the North Atlantic circulation. *The Johns Hopkins Oceanographic Studies*, *6*, 110.